Supplementary information for

The redistribution of anthropogenic excess heat is a key driver of warming in the North Atlantic

Marie-José Messias[1] and Herlé Mercier[2]

1. College of Life and Environmental Sciences, University of Exeter, Exeter EX4 4QE, United Kingdom.

2. University of Brest, Laboratoire d'Océanographie Physique et Spatiale, UMR 6523 CNRS/Ifremer/IRD/UBO, IUEM, Ifremer Centre de Brest, CS 10070, 29280 Plouzané, France.

Content of this supplementary information

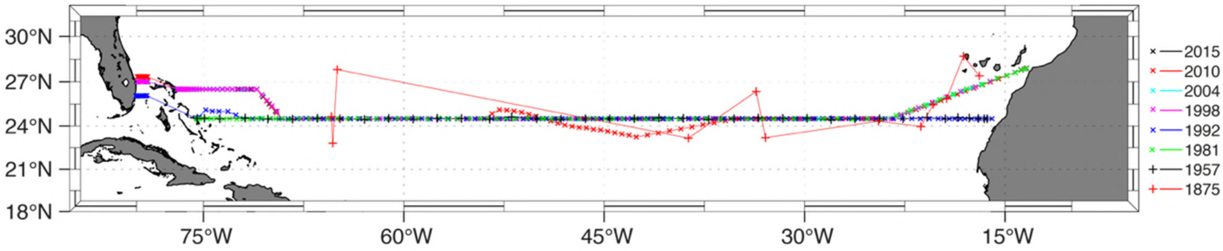

Supplementary Fig. 1: Cruise tracks. Tracks of the cruise used in this study. The time of the cruises are coded with markers and colours according to the insert: x and black for 2015, red for 2010, cyan for 2004, blue for 1992, green for 1981, magenta for 1998, and + and black for 1957, red for 1875. The main differences between the cruise tracks are: the trans-Atlantic section crossed the western boundary current further north from 1998 and its eastern side was deviated northward in 1981 and from 1998. The trans-Atlantic cruise tracks were complemented by a section in the Florida Strait from 1992. The 2010 trans-Atlantic section was deviated through the Mid-Atlantic Ridge Kane Fracture Zone. The 1875 stations are extracted from the 1873-1876 Challenger expedition. Corrections were applied to compensate for the bias due to the different sampling locations e.g., cold waters from the upwelling near the African coast (see Supplementary Note 1).

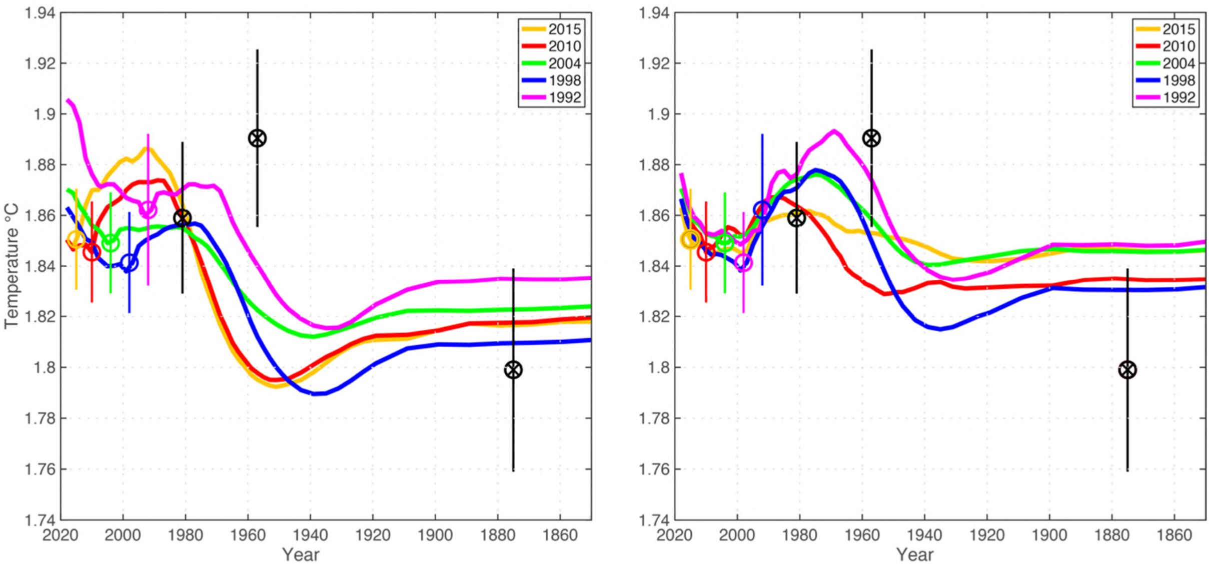

Supplementary Fig. 2: Temperature times series before and after Bayesian optimisation. This example is for the abyssal layer. The mean temperature is averaged along 25°N and for the depth layer 4000 m to bottom. The mean temperature evolutions are shown for each of the cruises used in this study to determine the Green's functions (2015, 2010, 2004, 1998, 1992, identified by colours as per the inserts). The comparison shows that the reconstructed times series using the Maximum Entropy Principle before the Bayesian adjustment are cruise specific, slightly shifted in time to exactly fit the cruise data and exhibiting a smoothed variability. The Bayesian optimisation uses all the cruise data together to constrained each reconstruction, aligning them in time and re-instating the observed variability. For the Bayesian adjustment, we used the cruises used to determine the Green's functions plus the 1981 and 1957 cruises which do not have transient and nutrients tracer data but have temperature and salinity (Supplementary information Table 1). Circles with error bars are average temperatures computed from the hydrographic measurements in colour for 2015, 2010, 2004, 1998 and 1992 and in black for 1981, 1957 and 1873. The 1873 data are from the Challenger Expedition and having a parse sampling are only reported here for comparison. See Supplementary Text 1 for details on how error bars on hydrography were computed.

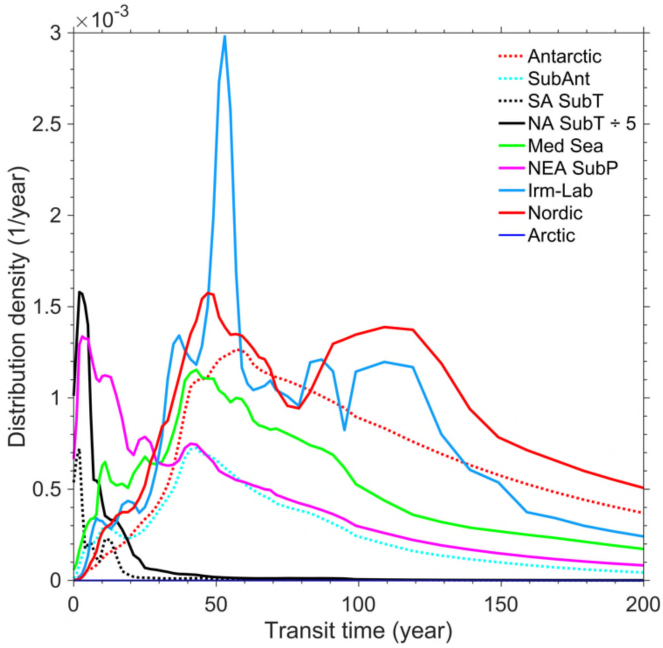

Supplementary Fig. 3: Age spectrums of the waters contributing to 25°N. Age spectrums are the time components of the Green's functions, zonally and vertically averaged for the full water column, and presented for the last 200 years. The age spectrum or transit time distribution characterises the complex interactions of advection and diffusion on all scales. The contributing waters are seen arriving with a modal age (maximum of the distribution) of 0-5 years for SA-SubT and NA-SubT, 10 years for NEA-SubP and 40-55 years for Lab-Irm, Nordic, Antarctic, Sub-Ant and Med Sea. It should be kept in mind in the interpretation that here the modal ages are for the full water column and for zonal averages spanning the well ventilated western boundary current and the eastern basin so include the impact of the memory of older climatic signals[1,2]. Interestingly, the increase in the density distributions between 7 to 14 years for the components of the NADW are a signature of the faster western boundary current and new replenishments of the water masses. The age spectrum for the Irm-Lab and the Nordic Seas transports are nearly bimodal, with a predominant mode at ~50 years and a older mode ~120 years, the latter likely a signature of the interior pathways and eastern basin routes[3]. The wide range of NEA SubP age spectrum highlights its fast contribution to the upper ocean as well as to the North Atlantic Deep Water by entrainment at the overflows. Note that NA-SubT distribution was divided by 5.

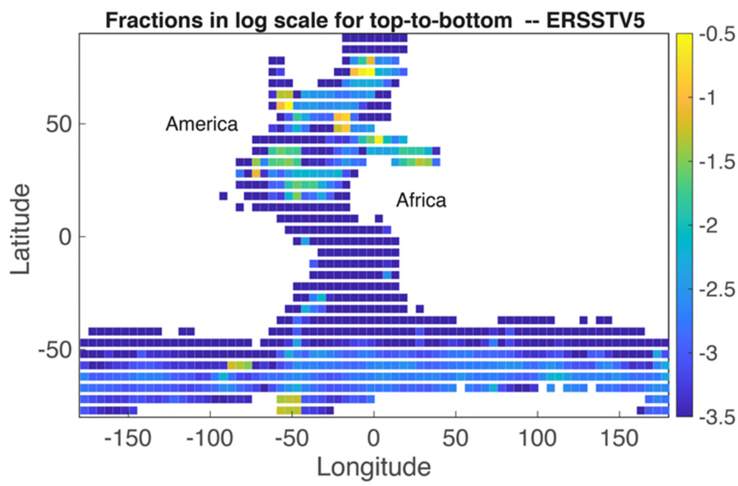

Supplementary Fig. 4: Map of 5° x 5° patch contributions to the tracer signal at 25°N. Contributions are reported in log-scale. This example describes how much the 5° x 5° patches contribute to the reconstruction of the surface-to-bottom tracer signal at 25°N.

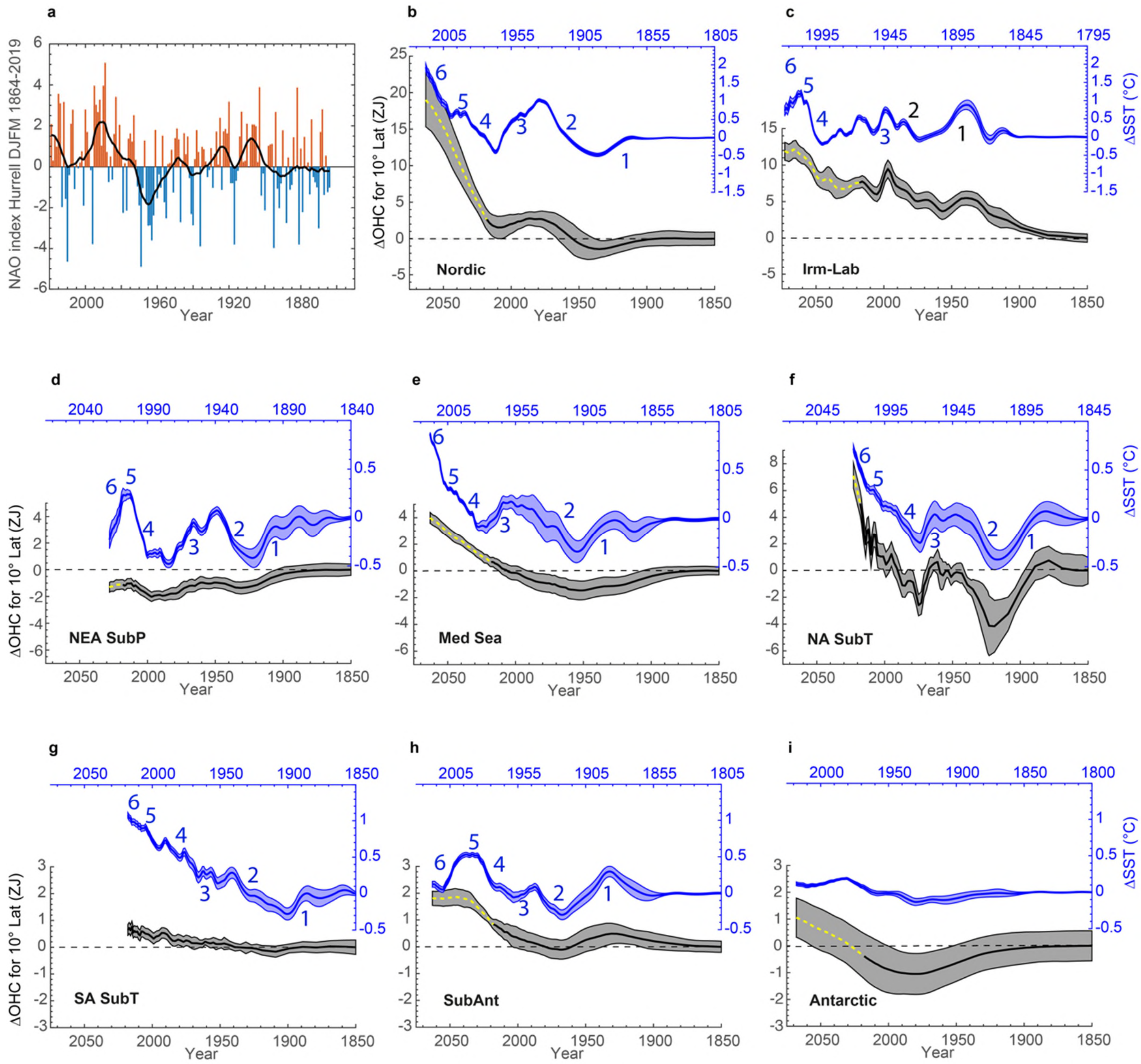

Supplementary Fig. 5: Historical contributions of all the source regions used in this study to full water column ΔOHC at 25°N and their future projections. As in main text Fig. 4, but completed here for the southern hemisphere contributing regions. Time series of NAO index (Data). **b**. Times series of the ΔSST (blue, right y-axis) and of the full depth ΔOHC response (black, left y-axis) for the Nordic source region defined in Fig. 3a. The ΔSST are weighted by their spatial and monthly contributions to the full water column at 25°N, and a low-passed filtered using a 10-year moving mean. The ΔSST time axis is shifted backward in time by the modal transit time to highlight the correspondence between ΔSST and ΔOHC. The GFs potential to infer the interior signal from past ΔSST is also used to project ΔOHC in the future over a time span equal to the modal transit time (yellow dotted line), assuming no change in the average circulation constrained here by the five hydrographic surveys from 1992 to 2016. ΔSST were regionally averaged over 5° x 5° patches weighted by their corresponding contributions to ΔOHC. **c**, **d**, **e**, **f**, **g**, **h**, **i.** same as for **b** but for Lab-Irm, NA-SubT, Med-Sea, NEA-SubP, SA-SubT, Sub-Ant and Antarctic regions. Note the different y-scales. The sum of ΔOHC from the 8 regions in panel **b**-**i** is the surface to bottom ΔOHC in Fig. 2b. Six climatic epochs discussed in the paper are indicated by numbers as follows: **1.** the late 1800's cooling, **2.** the early-twentieth-century warming, **3.** the mid-twentieth-century cooling, **4.** the late-twentieth-century warming, **5.** the early-twenty-first-century slowdown, and **6.** the early-twenty-first-century acceleration.

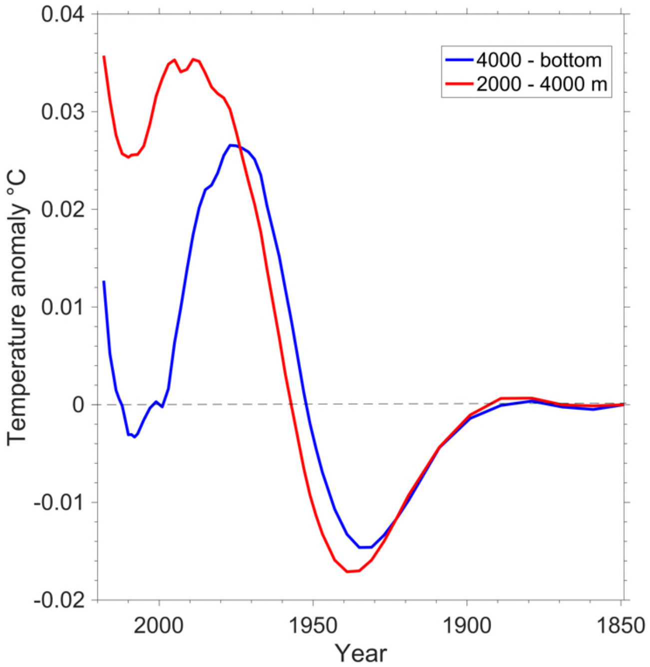

Supplementary Fig. 6: Time series of the Nordic contribution to ΔT at 25°N for the deep and the abyssal layer. The Nordic ΔT contribution to the 4000 m–bottom (blue) and 2000–4000 m (red) layers show comparable patterns however for the recent reversal to a cooling occurred well earlier in the abyssal layer (1987) and is stronger. This is attributed to the predominance in the abyssal layer of younger Denmark Strait Overflow Water that reaches 25°N with shorter transit times than the overlaying Iceland-Scotland Overflow Water.

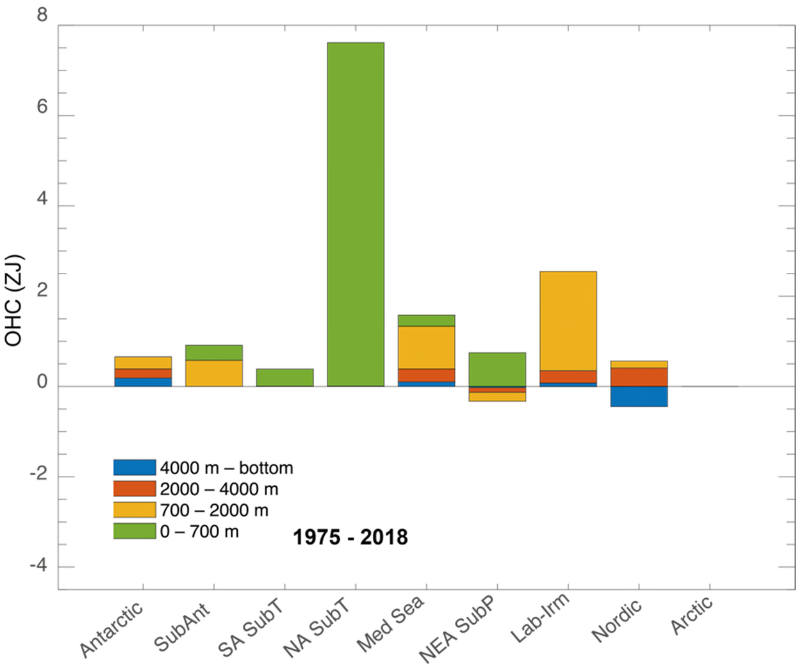

Supplementary Fig. 7: Source regions and their contributions to ΔOHC at 25°N in 2018 relative to 1975. As in main text Fig. 2c, but relative here to 1975 instead of 1850. The different regions are those represented in Fig. 3a of the main text. Colours refer to different depth ranges: 0–700 m (green), 700–2000 m (yellow), 2000–4000 m (red), 4000m–bottom (blue).

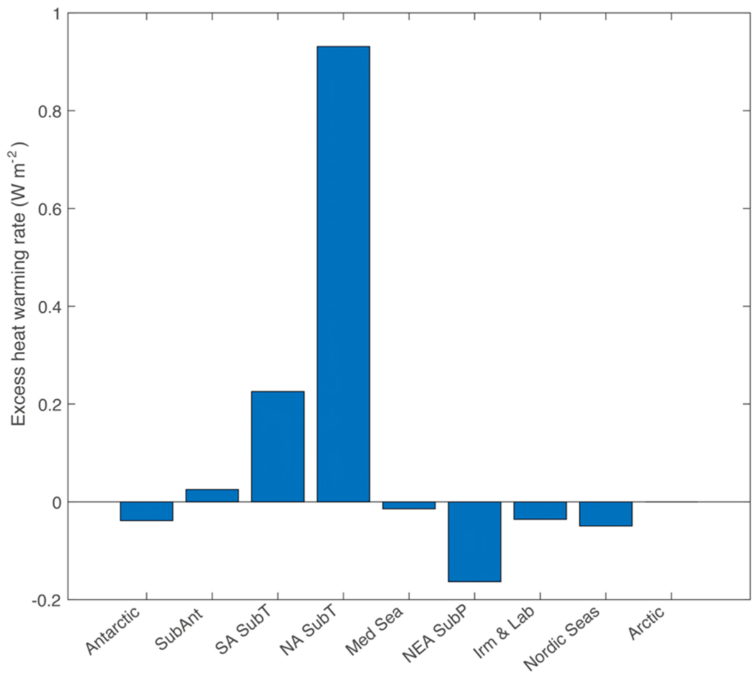

Supplementary Fig. 8: Regional contributions to the transport of excess heat across 25°N expressed as a warming rate north of the 25°N. The 9 contributors are the Arctic (negligeable), the Nordic Seas (Nordic), the Labrador and Irminger Seas (Lab-Irm), the north-eastern subpolar Atlantic (NEA-SubP), the Mediterranean Sea (Med Sea), the tropical and subtropical north Atlantic (NA-SubT), the tropical and subtropical South Atlantic (SA-SubT), the Sub-Antarctic (SubAnt) and the Antarctic. The warming rate is the 2012–2018 average. The domain is between the 25°N and the Bering Strait.

Cruise / Ship Expocode	**Period**	**Station Number**	**Variables used**
Challenger	1873-1876	21	Temperature and depth
Discovery II	6 Oct. – 7 Dec. 1957	38	Hydrography (salinity, temperature and depth)
Atlantis II	11 Aug. – 6 Sep. 1981	90	Hydrography CTD
HE06 / Hesperides 29HE06_1	14 Jul. – 15 Aug. 1992	112	Hydrography CTD, nitrate, phosphate, dissolved oxygen, CFC-11, CFC-12
R.H. Brown 31RBOACES24N_2	23 Jan. – 23 Feb. 1998	130	Hydrography CTD, nitrate, phosphate, dissolved oxygen, CFC-11, CFC-12
Discovery 74DI20040404	4 Apr. – 10 May 2004	125	Hydrography CTD, nitrate, phosphate, dissolved oxygen, CFC-11, CFC-12
D346 / Discovery 29AH20110128	6 Jan. – 18 Feb. 2010	135	Hydrography CTD, nitrate, phosphate, dissolved oxygen, CFC-11, CFC-12, SF_6
DY040 / Discovery 74EQ20151206	6 Dec 2015 – 22 Jan. 2016	145	Hydrography CTD, nitrate, phosphate, dissolved oxygen, CFC-11, CFC-12, SF_6

Supplementary Table 1: Cruises details. Repeat hydrography datasets at 25°N used in this study, also known as hydrographic line A05 used in this study. CTD stands for conductivity–temperature–depth.

Supplementary Note 1: Errors on excess temperature estimates from hydrographic cruises.

The coast-to-coast mean temperature and associated error were computed for each of the 7 hydrographic cruises and each of the 4 layers (Fig.2 and Supplementary Figure 3). Different sources of errors were identified.

First, the 7 hydrographic tracks are not all the same (Figure S2). The years 1957 and 1992 are along 25°N, 1981 departs from 25°N at the eastern boundary and 2004, 2010 and 2015 depart from 25°N both at the eastern and western boundaries. The year 2010 deviates from 25°N near the Mid-Atlantic Ridge. We used all the 1873 HMS Challenger stations located between 18°N and 28.8°N to optimise the number of measurements usable and obtain averaged layer temperatures that can be taken as representative and reasonably compared to those of the A05 surveys. Doing so, we use 21, 20, 16 and 5 stations for the layer 0-700, 700-2000, 2000-4000 and 4000-bottom, pondering by distance between stations for the average. Although coarsely spaced, the well-thought sampling during the Challenger expedition provides deep measurements at five stations in main sub-sections, which are the western boundary current, the western basin, the western side of the Mid-Atlantic Ridge, the eastern side of the Mid-Atlantic Ridge and the eastern boundary current. Cruise tracks for the years 1998 and 2004, which were the same, were taken as reference. Mean temperatures in layers are affected by bias due to these different tracks and the different spatial resolution of the hydrographic sections. These biases were corrected by estimating differences in layer-average temperature between the original and the reference cruise track in EN4 for the period 2006-2018 when data from the Argo program were available. For example, we obtain a cold bias of 0.06°C for the 700-2000 m layer and the 1957 and 1992 cruise track which does not deviate northwards near the African coast as for the other cruises, and instead continue eastward into the upwelling. The second source of error that we considered was the seasonal bias that was also computed from EN4 along the reference cruise track. The total errors reported in Supplementary Figure 3 were exclusively used in the Bayesian minimisation process (Equation 4).

Supplementary Note 2: Region definitions.

The nine regions in Fig.3 (main text) were selected after some trials to account for all the contributing regions to the 25°N water masses and keep computational time reasonable. Where results were insensitive to a surface region, the corresponding patches were put under the label “Other”. Those include the patches in the Pacific Ocean and the Indian Ocean north of the regions of formation of the Antarctic Intermediate Water (latitude north of 30°S for the Pacific Ocean, latitude north of 24°S for the Indian Ocean), and in the Arctic Ocean with the exception of the western Eurasia Basin.

Supplementary Note 3: Discretisation.

We discretized the Green’s functions following ref.[4,5]. Thus, the Green’s functions were written as $\mathcal{G}(s, \mathrm{m}, \mathrm{n})$ where the index of the surface patches s refers to the 5° x 5° surface patches where surface properties are defined, the index of the years m refers to the time period from year 1 to year 2018 with an uneven sampling varying from 1 year between 2018-2008, 2 years between 2007-1947, 4 years between 1943-1919, 10 years between 1909-1701 and 100 years until year 1. The index of the months n varies from 1 to 12. The normalization is such that the integration over the regions, years and months of the Green’s functions is equal to 1.

Supplementary References

1. Wunsch, C. & Heimbach, P. Bidecadal Thermal Changes in the Abyssal Ocean. *J. Phys. Oceanogr.* **44**, 2013–2030 (2014).
2. Gebbie, G. Atlantic Warming Since the Little Ice Age. *Oceanography* **32**, 220–230 (2019).
3. Paillet, J. & Arhan, M. Oceanic Ventilation in the Eastern North Atlantic. *J. Phys. Oceanogr.* **26**, 2036–2052 (1996).
4. Holzer, M., Primeau, F. W., Smethie Jr., W. M. & Khatiwala, S. Where and how long ago was water in the western North Atlantic ventilated? Maximum entropy inversions of bottle data from WOCE line A20. *J. Geophys. Res. Ocean.* **115**, (2010).
5. Ting, Y.-H. & Holzer, M. Decadal changes in Southern Ocean ventilation inferred from deconvolutions of repeat hydrographies. *Geophys. Res. Lett.* **44**, 5655–5664 (2017).